The innate immune receptor TREM-1 promotes liver injury and fibrosis

Anh Thu Nguyen-Lefebvre[1], Ashwin Ajith[1], Vera Portik-Dobos[1], Daniel David Horuzsko[1], Ali Syed Arbab[2], Amiran Dzutsev[3], Ramses Sadek[4], Giorgio Trinchieri[3], and Anatolij Horuzsko[1,5]

[1]Molecular Oncology and Biomarkers Program, Georgia Cancer Center, Department of Medicine, Medical College of Georgia, Augusta University, Augusta, Georgia, USA.

[2]Tumor Angiogenesis Laboratory, Georgia Cancer Center, Department of Biochemistry and Molecular Biology, Augusta University, Augusta, Georgia, USA.

[3]Cancer and Inflammation Program, Center for Cancer Research, National Cancer Institute, National Institutes of Health, Bethesda, Maryland, USA.

[4]Georgia Cancer Center, Augusta University, Augusta, Georgia, USA.

[5]Corresponding author: Anatolij Horuzsko, Molecular Oncology and Biomarkers Program, Georgia Cancer Center, Department of Medicine, Medical College of Georgia, Augusta University, 1410 Laney Walker Blvd, Augusta, Georgia, 30912, USA.

Phone: 706.721.8736; Fax: 706.721.0101. E-mail: ahoruzsko@augusta.edu

Keywords: liver injury; liver fibrosis; inflammation; Kupffer cells; hepatic stellate cells; inflammatory monocytes.

Note: Supplemental material is available for this manuscript.

Electronic word count: 8456 words including the abstract, references, and figure legends.

Number of figures: 8 figures.

Number of supplemental figures and table: 17 figures; 1 table.

Conflict of interest: The authors have declared that no conflicts of interest exist.

Abstract

Inflammation occurs in all tissues in response to injury or stress and is the key process underlying hepatic fibrogenesis. Targeting chronic and uncontrolled inflammation is one strategy to prevent liver injury and fibrosis progression. Here, we demonstrate that triggering receptor expressed on myeloid cells-1 (TREM-1), an amplifier of inflammation, promotes liver disease by intensifying hepatic inflammation and fibrosis. In the liver, TREM-1 expression is limited to liver macrophages and monocytes and is highly upregulated on Kupffer cells, circulating monocytes, and monocyte-derived macrophages in a mouse model of chronic liver injury and fibrosis induced by carbon tetrachloride (CCl_4) administration. TREM-1 signaling promotes pro-inflammatory cytokine production and mobilization of inflammatory cells to the site of injury. Deletion of *Trem1* reduced liver injury, inflammatory cell infiltration, and fibrogenesis. Reconstitution of *Trem1*-deficient mice with *Trem1*-sufficient Kupffer cells restored recruitment of inflammatory monocytes and severity of liver injury. Markedly increased infiltration of liver fibrotic areas with TREM-1-positive Kupffer cells and monocytes/macrophages was found in patients with hepatic fibrosis. Our data support a role of TREM-1 in liver injury and hepatic fibrogenesis and suggests that TREM-1 is a master regulator of Kupffer cell activation, which escalates chronic liver inflammatory responses, activates hepatic stellate cells, and reveals a novel mechanism of promotion of liver fibrosis.

Introduction

Fibrosis is a highly evolved defense response resulting in encapsulation of an injury in adult tissue. Hepatic fibrosis occurs in diseases associated with chronic liver injury and hepatocellular death, e.g., viral hepatitis, alcohol abuse, and drugs or chemical insults (1-6).

The liver is a target of infectious pathogens that via microbial-associated molecular pattern (MAMP) molecules induce an inflammatory response (7). In acute liver infections, inflammatory cell infiltration and hepatocellular damage are observed (8, 9). Repetition and/or persistence of the injury induces an extensive chronic inflammatory reaction in the liver resulting in a scarring process that destroys the normal architecture of the organ, leading to fibrosis and cirrhosis (10). In addition to infection-attributable fibrosis, liver fibrosis also occurs in response to a wide range of stimuli that cause stress and injury leading to sterile chronic inflammation (11, 12).

Although inflammation is correlated with fibrosis progression (1, 13, 14), the cellular and molecular mechanisms that promote liver injury and fibrogenesis remain enigmatic. The triggering receptor expressed on myeloid cells-1 (TREM-1) is involved in the control of acute and chronic inflammatory responses. TREM-1 is a cell surface activating receptor and a member of the immunoglobulin superfamily that potently amplifies inflammatory responses by inducing the secretion of inflammatory mediators (15). TREM-1 is expressed on neutrophils, monocytes and macrophages, where it is upregulated during infection, cancer development and following Toll-like receptor (TLR) engagement (16, 17). TREM-1 has a V-type extracellular domain, a charged transmembrane domain, and a short cytoplasmic tail. TREM-1 associates with the adaptor molecule DAP12, which is required for surface expression and signaling by TREM-1 (18). DAP12 mediates downstream signaling through a cytoplasmic ITAM

domain, which recruits SYK and activates PI3K, phospholipase C, and Vav signaling (16, 19). Limited data are available on the role of TREM-1 in liver inflammation and fibrogenesis. TREM-1 is expressed in human tumor-activated hepatic stellate cells (HSCs), and its level of expression is a prognostic factor for poor survival in patients with hepatitis B-related hepatocellular carcinoma (HCC), an inflammation-associated malignancy (20).

Recently, we have demonstrated that TREM-1 is instrumental for Kupffer cell activation in a diethylnitrosamine-induced model of liver carcinogenesis and that its deletion attenuates development of HCC (21). Here, we provide the first evidence that TREM-1 signaling, by targeting a chronic inflammatory response and pro-fibrogenic pathways, is essential for inducing inflammatory-mediated liver injury and fibrogenesis. We determined that Kupffer cells play a fundamental role in chronic liver inflammation and fibrogenesis using a model for liver fibrosis induced by repetitive injections of carbon tetrachloride (CCl_4). This well-defined and characterized model of chronic liver damage shares many features of chronic liver diseases in humans, including the development of liver fibrosis (22). TREM-1 has limited expression in healthy human liver. In contrast, in liver fibrotic areas from patients with advanced hepatic fibrosis the number of TREM-1-positive liver macrophages and monocytes was markedly increased. In this study, we describe a novel TREM-1-mediated mechanism of liver injury and fibrogenesis.

Results

TREM-1 enhances development of liver fibrosis.

A single dose of CCl_4 induces centralobular necrosis and reversible injury that triggers a wound-healing response (23). Repetitive administration of CCl_4 promotes progressive fibrogenesis, cirrhosis, and finally HCC. To determine the role of TREM-1 in liver injury and fibrogenesis, *Trem1*$^{-/-}$ and wild-type (WT) mice were injected with 12 doses of CCl_4 over a 6-week period that in WT mice induce marked hepatic fibrosis. *Trem1*$^{-/-}$ mice showed significantly less fibrosis than WT mice, as analyzed by i) macroscopic appearance, ii) collagen deposition (Sirius red staining, 12.2% ± 1.5% positive area for WT mice, 6.3% ± 0.5% for *Trem1*$^{-/-}$ mice), and iii) expression of α-smooth muscle actin (α-SMA) (immunohistochemistry, 33.7% ± 1.6% for WT mice and 17.2% ± 1.5% for *Trem1*$^{-/-}$ mice, Figure 1, A-E). A significant decrease of hepatic α-SMA expression in *Trem1*$^{-/-}$ mice compared to WT mice was also observed by immunoblot analyses of total liver proteins (Figure 1, F and G). We also examined fibrosis development using Bismuth Oxide Nanoparticles (Mvivo BIS), a contrast agent designed for small animal liver micro-CT imaging. Following administration, low doses of MvivoBIS are rapidly taken up by the reticuloendothelial system in the liver, enabling high definition imaging. After 6 weeks of CCl_4 treatment, WT mice showed significantly less uptake of MvivoBIS nanoparticles in liver than *Trem1*$^{-/-}$ mice (Supplemental Figure S1, A and B). Alanine aminotransferase (ALT) and aspartate aminotransferase (AST) activities were measured as indicators of CCl_4-induced liver injury. Both groups of mice demonstrated elevated ALT and AST levels at 6 weeks after CCl_4 treatment. However, ALT and AST levels increased more than 2-fold and 3-fold, respectively, in WT mice at week 6, while no significant increase was seen in *Trem1*$^{-/-}$ mice, indicating a greater sensitivity for the development of liver injury in WT mice (Supplemental Figure S2). CCl_4-treated WT mice showed a

significantly higher level of expression of fibrogenic genes that are upregulated in hepatic fibrosis than *Trem1*$^{-/-}$ mice, including α1 type 1 collagen (*Col1a1)*, α2 type 1 collagen (*Col1a2)*, α1 type 3 collagen (*Col3a1),* α1 type 5 collagen (*Col5a1),* TGF-β1 *(Tgfb1),* and α-SMA (*Acta2*) (Supplemental Figure S3)**.**

TREM-1 is essential for hepatic stellate cell activation.

HSCs are the major collagen-producing cells in the fibrotic liver (1). Upon chronic liver injury, HSCs are activated to promote fibrogenesis by a wide range of signals from injured hepatocytes, activated Kupffer cells, inflammatory cells, and liver sinusoidal endothelial cells (LSECs). Upon activation, HSCs release vitamin A and lipid droplets and differentiate into myofibroblasts, elongated cells with fibrogenic and contractile activities (24, 25). In control (oil-treated) WT and *Trem1*$^{-/-}$ mice, HSCs exhibit a quiescent phenotype and store vitamin A and lipid droplets, which display fading blue-green autofluorescence when excited with a light of ≈ 405-407 nm and detected with a 450/50 nm band-pass filter (26) (Figure 2A, upper panels). After 12 doses of CCl_4, HSCs from WT mice displayed characteristics of activated HSCs (Figure 2A, lower left panel). In contrast, most HSCs from CCl_4-treated *Trem1*$^{-/-}$ mice maintained a non-activated vitamin A-rich round morphology (Figure 2A, lower right panel). The role of TREM-1 in HSC activation was confirmed by the observation that mRNA expression of genes upregulated during cell activation and fibrogenesis (*Col5a1*, *Acta2*, *Mmp10,* and *Timp1*) was significantly higher in CCl_4-treated WT mice than in *Trem1*$^{-/-}$ mice (Figure 2B). Conversely, the transcript levels of genes that are downregulated in activated HSCs (*Hhip* encoding hedgehog interacting protein and *Plxnc1* encoding plexin C1) were lower in CCl_4-treated WT mice than in *Trem1*$^{-/-}$ mice (Figure 2C).

TREM-1 enhances hepatic inflammation during fibrogenesis.

Treatment of WT mice with 12 doses of CCl_4 elicited extensive changes in liver morphology, as observed on hematoxylin and eosin-stained tissue sections, including significantly increased cell infiltration surrounding islands of hepatocytes. In contrast, CCl_4-treated *Trem1*$^{-/-}$ mice showed significantly reduced hepatic cell infiltration in comparison with WT mice (Figure 3, A and B). Fluorescent immunohistology showed after CCl_4 treatment a substantially lower number of F4/80-positive cells in the liver of *Trem1*$^{-/-}$ mice than in WT mice (Figure 3C). Non-parenchymal cells isolated from WT and *Trem1*$^{-/-}$ livers were analyzed by flow cytometry to evaluate the CCl_4-induced accumulation of myeloid cells that are required for HSC activation and hepatic fibrosis (27). While the number of cells expressing the pan-myeloid marker CD11b was similarly upregulated in both mouse strains by CCl_4 treatment, the number of F4/80$^+$ cells was markedly reduced in CCl_4-treated *Trem1*$^{-/-}$ mice compared to WT mice (Figure 3, D and E). Liver-associated F4/80$^+$ cells were composed of two populations: F4/80$^+$CD11b$^-$, corresponding to resident Kupffer cells, and F4/80$^+$CD11b$^+$ cells. Analysis of the cell surface markers Ly6C and Ly6G determined that most F4/80$^+$CD11b$^+$ cells were inflammatory monocyte-derived macrophages (F4/80$^+$CD11b$^+$Ly6C^{high}Ly6G^{low}) at different stages of differentiation (Figure 3D). The number of Kupffer cells and F4/80$^+$CD11b$^+$ cells was not significantly different in the livers of untreated WT and *Trem1*$^{-/-}$ mice but after CCl_4 treatment, the number of both cell types increased and reached significantly higher levels in WT mice than in *Trem1*$^{-/-}$ mice (Figure 3E). Most F4/80$^-$CD11b$^+$ cells express a high level of surface Ly6G (Ly6G^{high}Ly6C^{low}) (Figure 3D) that identified them as neutrophils. These neutrophils were increased by CCl_4 treatment similarly in WT and *Trem1*$^{-/-}$ mice (Figure 3E). The significant increase of monocyte-derived macrophages (F4/80$^+$CD11b$^+$) in CCl_4-treated WT mice compared to *Trem1*$^{-/-}$ mice was confirmed in situ using a fluorescent multiplexed immunohistochemistry assay

(Supplemental Figure S4, A and B). In both groups of CCl_4-treated mice, the abundancy of adaptive immune cells such as T cells ($CD4^+$, $CD8^+$) and B cells ($B220^+$) was minimal (Supplemental Figure S4C). These data demonstrate that during fibrosis development TREM-1 signaling modulates myeloid hepatic inflammation inducing an increased accumulation of monocyte-derived macrophages and resident Kupffer cells while it does not affecting the number of neutrophils.

TREM-1 controls mobilization of inflammatory cells in response to injury and consequently enhances liver damage.

To analyze the role of TREM-1 in mediating the recruitment of inflammatory cells during fibrogenesis, we examined the early stage of CCl_4-induced liver injury. CCl_4 is quickly metabolized by liver cytochrome P450 enzymes into trichloromethyl free radicals that initiate a lipid peroxidation chain reaction leading to hepatocyte death and liver damage (28). Necrotic hepatocytes release damage-associated molecular pattern (DAMP) signaling molecules, including high mobility group box 1 (HMGB1) protein and HSP70, that induce activation, proliferation, and recruitment of inflammatory cells (21, 29-32), thus amplifying liver injury and establishing chronic inflammation. Both liver-resident cells and cells that are recruited in response to injury produce pro-inflammatory signals that contribute to the apoptotic and necrotic damage of hepatocytes. Injection of a single dose of CCl_4 increases ALT and AST activities almost equivalently in WT and *Trem1*$^{-/-}$ mice at 6 h and 12 h (Figure 4, A, B, D, and E). However, while these increased levels were maintained in WT mice, they decreased and were reduced to the level of untreated mice at 72 h in *Trem1*$^{-/-}$ mice (Figure 4, C and F). These data indicate that TREM-1 signaling contributes to the persistency of the inflammatory response following CCl_4 treatment and enhances liver injury.

The bone marrow is one of the sensors of liver injury. A single dose of CCl_4 treatment induced only a modest perturbation of the number of total $CD11b^+$ cells, neutrophils, and monocytes in the bone marrow of *Trem1*$^{-/-}$ mice and WT mice (Supplemental Figures S5, A-D, and S6A). Analysis of peripheral blood cells showed that 12 h after CCl_4 treatment a similar increase of CD11b-positive myeloid cells including neutrophils and monocytes was observed in both mice. However, 72 h after CCl_4 treatment, the frequency of myeloid cells in the blood was significantly higher in WT mice than in *Trem1*$^{-/-}$ mice (Supplemental Figure S5, F-H, and S6B). A much higher blood accumulation of patrolling monocytes ($CD11b^+F4/80^+CCR2^-CX3CR1^+$) cells (33) was also induced by CCl_4 injection in WT mice than in *Trem1*$^{-/-}$ mice (Supplemental Figure S5H). The most dramatic changes, however, were observed in livers of CCl_4-treated mice. The number of myeloid cells, and especially neutrophils (Supplemental Figure S6C), progressively increased at both 12 h and 72 h and was at a significantly higher level in the livers from WT mice than *Trem1*$^{-/-}$ mice (Figure 5, A-C). The number of monocyte-derived macrophages ($CD11b^+F4/80^+Ly6C^{high}$) (Supplemental Figure S6C) was greatly increased in the injured livers from WT mice but they were almost absent in *Trem1*$^{-/-}$ mice (Figure 5D). These cells were $CCR2^+CX3CR1^{low}$ and produced IL-1β, TNF, and TGF-β1 (Figure 5A), which characterized them as infiltrating inflammatory monocyte-derived macrophages (34). Expression of genes involved in recruitment and maintenance of inflammatory cells, including *Ccl2, Ccl7, Cxcl10, Tnf, Il1b* and *Il6,* was induced by CCl_4 (12 h and 72 h after CCl_4 injection) in the liver of WT mice but not of *Trem1*$^{-/-}$ mice (Supplemental Figure S7). Thus, our data reveal a key role of TREM-1 in mobilization, recruitment and differentiation of inflammatory cells to the site of inflammation and injury.

Increased expression of TREM-1 in liver and pro-fibrogenic signature of activated Kupffer cells during fibrogenesis.

Total RNA was isolated from livers of oil- or CCl_4-injected WT mice and analyzed by RT-qPCR. *Trem1* mRNA accumulation was increased at 12 h, 72 h and 6 weeks after CCl_4 treatment, with a maximum of 20-fold induction at 12 h (Figure 6A). The protein level of TREM-1 in liver was also increased by CCl_4 injection with a peak at 72 h (Figure 6, B and C). Fluorescent immunostaining of liver from WT mice at different time points confirmed the increase of TREM-1 in response to CCl_4 (Figure 6D). To determine the cell types that express TREM-1 in normal liver, RT-PCR was performed on total RNA isolated from whole liver, purified hepatocytes, Kupffer cells, and HSCs of WT mice; only Kupffer cells were observed to express *Trem1* (Figure 6E). Flow cytometry analysis confirmed that TREM-1 protein was present only on Kupffer cells, and its density on these cells was increased at 12 h and even more at 72 h in CCl_4-induced liver injury (Figure 6, F and G). The increased level of TREM-1 expression on Kupffer cells following CCl_4 treatment may be responsible for their production of inflammatory chemokines, cytokines, and growth factors.

RNA sequencing data showed that CCl_4 treatment of WT mice resulted in a major shift of the transcriptome profile of Kupffer cells, with about 1000 genes differentially expressed of which about 360 were increased and 640 decreased. Interestingly, the large majority of the genes that were induced or decreased by CCl_4 treatment in WT mice were not modified or were modified to a significantly lesser degree than in *Trem1*$^{-/-}$ mice (Supplemental Figure S8A). The similarity between Kupffer cells from untreated WT mice and CCl_4-treated *Trem1*$^{-/-}$ mice is further demonstrated by correlation analysis of log2 transformed ratios of Kupffer cell transcripts from CCl_4-treated WT mice vs ones from CCl_4-treated *Trem1*$^{-/-}$ mice or untreated WT mice. The R-value between the two ratios was 0.76 with p value $<10^{-4}$. Among the genes encoding growth factors that were

upregulated by Kupffer cells in WT but not in *Trem1*$^{-/-}$ mice after CCl_4 treatment were factors already shown to play a role in liver fibrosis, such as *Tgfb1, Jag1* (jagged 1), and *Osm* (oncostatin M), as well as other factors, such as *Btc* (betacellulin, a member of the epidermal growth factor family), *Agt* (angiotensinogen), *Inhba* (inhibin beta A) and *Mst1* (macrophage stimulating 1, hepatocyte growth factor-like). The expression of genes encoding cytokines and chemokines was upregulated in WT mice, but not in *Trem1*$^{-/-}$ mice. These included the cytokine gene *Il23a* and the chemokine genes *ccl9*, *cxcl2* and *cxcl3*, whose expressed proteins for attract inflammatory and immune cell migration *via* CCR1 and CXCR2, and affect their processes of differentiation and function (Supplemental Figure S8B). In addition, total liver expression of TGF-β1 is significantly higher in WT mice compared with *Trem1*$^{-/-}$ mice (Supplemental Figure S9). These data support that TGF-β1 is the major regulator of liver fibrogenesis. A significant decreased level of production of TNF and TGF-β1 was determined in Kupffer cells from *Trem1*$^{-/-}$ mice at 72 h after CCl_4 injury, as shown in Figure 6, H and I. Lack of upregulation of the *Ccl9*, *Cxcl2*, *Cxcl3, Il1f9,* and *Il23a* genes as well as the decreased levels of TNF and TGF-β1 in *Trem1*$^{-/-}$ mice suggest that deletion of the *Trem1* gene alters Kupffer cell activation during the CCl_4-induced inflammatory response.

Adoptive transfer of Trem1-sufficient Kupffer cells to Trem1-deficient mice reconstitutes their impaired myeloid inflammatory response following CCl_4-induced injury.

To test whether the impaired activation of Kupffer cells in *Trem1*$^{-/-}$ mice plays a major role in the reduced response of liver injury and recruitment of inflammatory cells to CCl_4-induced liver damage, Kupffer cells were depleted in WT and *Trem1*$^{-/-}$ mice by treatment with chlodronate-containing liposomes (Figure 7A, upper panels), followed by

intravenous reconstitution with Kupffer cells isolated from WT mice and CCl_4 injection (Figure 7A, lower panels). A similar number of transferred Kupffer cells migrated at 18 h into the liver of depleted WT and *Trem1*$^{-/-}$ recipient mice. *Trem1*$^{-/-}$ mice in which *Trem1*-sufficient Kupffer cells were transferred recovered the ability to increase serum ALT and AST enzymes at 72 h after CCl_4 injection at comparable levels as observed in WT mice (Figure 4, C and F, and Figure 7, B and C). Adoptively transferred *Trem1*-sufficient Kupffer cells produced comparable amounts of TNF and TGF-β1 in WT and *Trem1*$^{-/-}$ recipient mice following CCl_4 treatment (Figure 7, D-F). The recruitment of peripheral blood neutrophils after CCl_4 treatment was comparable between *Trem1*$^{-/-}$ and WT mice reconstituted with *Trem1*-sufficient Kupffer cells (Supplemental Figure S10, A and B). Also, CCl_4 treatment of *Trem1*$^{-/-}$ mice reconstituted with *Trem1*-sufficient Kupffer cells induced a similar increase in the number of $CD11b^+F4/80^+$ patrolling monocytes/macrophages at 72 h as observed in CCl_4-injured WT mice (Supplemental Figure S10, A and C). The number of inflammatory monocytes and neutrophils recruited at 72 h post-CCl_4 treatment to the livers of *Trem1*$^{-/-}$ mice reconstituted with *Trem1*-sufficient Kupffer cells was comparable to that observed in WT mice, although lower compared to WT mice reconstituted with *Trem1*-sufficient Kupffer cells (Figure 7, D, G-H). Conversely, adoptive transfer of *Trem1*-deficient Kupffer cells into WT mice resulted in reduced CCl_4-induced liver injury and altered recruitment of neutrophils as well as of patrolling and inflammatory monocytes/macrophages (Supplemental Figure S11, A-H). These data indicate that transferred *Trem1*-sufficient Kupffer cells were activated in *Trem1*$^{-/-}$ mice in response to CCl_4 exposure and could induce liver injury while the transfer of *Trem1*-deficient Kupffer cells into WT mice protected them from CCl_4-induced liver injury.

Increased infiltration of liver with TREM-1-positive cells, including Kupffer cells and monocytes/macrophages in patients with hepatic fibrosis.

Human liver tissues from a control group (n = 6) and patients with liver fibrosis (n = 5) were analyzed for fibrosis biomarkers, TREM-1 expression, and phenotype. Collagen deposition, evaluated by Masson Trichrome staining, and level of α-SMA expression, were significantly increased in patients with advanced liver fibrosis (Figure 8, A, B, C left panels and D, and Supplemental Figures S12 and S13). In normal liver, most TREM-1-positive cells were found in and around the hepatic sinusoid, which is the primary location of Kupffer cells and of the morphologically and functionally unique LSECs (Figure 8C, middle and right panels). Since LSECs play a major role in liver regeneration after liver injury, it will be interesting to determine the role of TREM-1 in LSEC functions, especially in their crosstalk with HSCs during fibrogenesis. Healthy (non-capillarized) LSECs prevent and reverse activation of HSCs (35, 36). However, during fibrosis, capillarized LSECs lose the ability to antagonize HSC activation (36). A similar number of TREM-1-positive cells was detected in normal liver tissues from the control group and in non-fibrotic areas from patients with advanced liver fibrosis (31.47% ± 13.47% and 27.25% ± 6.8%, respectively) (Figure 8C middle panels). In contrast, an increase in the number of TREM-1-positive cells was observed in fibrotic areas compared with non-fibrotic areas (82.04% ± 9.68%, Figure 8, C middle panels and E, and Supplemental Figure S14). TREM-1-positive cells that express CD68, a marker of Kupffer cells were significantly increased in fibrotic areas (Figure 8, F and H, and Supplemental Figure S15). Other TREM-1-positive cells also markedly increased in fibrotic areas expressed the CD11b marker and were mostly markedly increased in fibrotic areas; the majority of these cells was represented by myeloid cells, including monocytes and monocyte-derived macrophages (Figure 8, F and G, and Supplemental Figure S16). Together,

these data suggest that human liver fibrosis is associated with recruitment/differentiation of both TREM-1-positive Kupffer cells and monocytes/monocyte-derived macrophages.

Discussion

Hepatic fibrosis is the consequence of liver damage produced by chronic infectious hepatitis, alcohol, or chemical insults (1-4). An excessive inflammatory response to the initial liver damage mediated by viruses or toxic metabolites amplifies the tissue damage, resulting in progression to chronic liver injury and fibrosis that eventually leads to cirrhosis and organ failure. Since fibrosis is preceded by an inflammatory response, targeting of both the innate and adaptive immune systems may provide powerful tools for therapeutic approaches to prevent, slow or even reverse fibrosis or cirrhosis (37, 38).

The TREM-1 signaling pathway has emerged as a central component of the liver's inflammatory response during acute and chronic liver injury. In this study, we have shown that the TREM-1-mediated response to the initial liver damage causes further injury to the liver and is linked to development of fibrosis. We focused in detail on the innate immune response to CCl_4-induced tissue damage and identified that the activation of TREM-1 in Kupffer cells plays a key role in initiation of the liver inflammatory response followed by HSC activation during fibrogenesis (Supplemental Figure S17). Kupffer cells are the major population of cells that express TREM-1 in the liver. During CCl_4-induced fibrogenesis, the expression of TREM-1 on Kupffer cells was enhanced early and maintained at levels higher than in untreated mice for the duration of the experiment. TREM-1 activation enhanced the inflammatory response to tissue damage, amplifying liver damage and leading to chronic inflammation. Recognition of HMGB1 by TREM-1 on Kupffer cells leads to production of pro-inflammatory cytokines (IL-1β, TNF, IL-6) that sensitize hepatocytes to apoptosis and necrosis (21, 29, 31, 32). Our study defines several crucial components of the TREM-1-mediated inflammatory response in the liver. The number of TREM-1-activated Kupffer cells and monocyte-

derived macrophages was markedly increased in fibrotic livers. The extensive recruitment of cells to the injured liver or/and survival and proliferation of resident cells could explain this finding (39, 40). There are conflicting results on the role of TREM-1 in prolongation of the life span of myeloid cells. Klesney-Tait et al. (41) demonstrated that TREM-1/3-deficient neutrophils undergo cell death at a similar rate as WT neutrophils, but they failed to migrate into the intrapulmonary airspace in a murine pneumonia model. In contrast, in various other models, TREM-1 blockade or deficiency was observed to inhibit cell proliferation directly or indirectly (21), suggesting that a full understanding of the role of TREM-1 in cell survival requires further investigation. Our study defines the recruitment of pro-inflammatory cells to the injured liver as one of the major mechanisms by which TREM-1 signaling on activated Kupffer cells establishes a chronic inflammatory response and enhances liver damage. *Trem1*-deficient Kupffer cells in CCl_4-treated mice fail to express genes such as *Ccl9*, *Cxcl2* and *Cxcl3* that encode chemokines involved in the recruitment, differentiation, and function of monocytes, neutrophils and macrophages (39, 40, 42-44). A high number of infiltrating pro-inflammatory monocytes and monocyte-derived macrophages recruited from bone marrow and peripheral blood to the area of injured pre-fibrotic and fibrotic livers was demonstrated in TREM-1-positive mice. Remarkably, reduced or absent infiltrating monocytes and monocyte-derived macrophages were observed in *Trem1*-deficient mice.

HSCs in normal healthy livers did not express TREM-1. There is increasing evidence that inflammation-related malignancy may trigger the expression of TREM-1 on tumor-activated HSCs (20). We did not detect *Trem1* expression on HSCs isolated from control (oil-treated) mice or during early stages of fibrogenesis in WT mice. However, we found upregulation of *Trem1* mRNA on activated HSCs in 50% of WT mice treated with CCl_4 for 6 weeks (data not shown). Since activation of HSCs occurs rapidly after liver injury, TREM-1 signaling is not the primary target on HSCs that drive fibrogenesis. Our

study provides several lines of evidence that TREM-1 signaling on Kupffer cells is the main target that drives fibrogenesis. Activated Kupffer cells from *Trem-1*$^{+/+}$ mice release various proinflammatory mediators, including the chemokine CCL9 as well as TGF-β1, which is considered the most powerful mediator of HSC activation (1, 13). Kupffer cells are the main source of TGF-β1 in the liver and promote HSC activation and fibrogenesis (13, 45). Several signaling pathways modulate hepatic inflammation and fibrogenesis. In particular, TLR4 enhances hepatic fibrosis through TGF-β1 signaling. The expression of TLR4 has been demonstrated on many cells in liver, including Kupffer cells and HSCs. *Tlr4*-deficent mice demonstrated markedly decreased fibrogenesis (13). However, chimeric mice containing *Tlr4*-deficient Kupffer cells demonstrated normal fibrogenesis (13). This data suggests that in Kupffer cells, TREM-1 rather than TLR4 plays a major role in promoting fibrogenesis. Moreover, adoptive transfer of *Trem1*-sufficient Kupffer cells into either *Trem1*$^{-/-}$ or WT mice resulted in similar CCl_4-induced liver injury. *Trem1*-sufficient Kupffer cells were activated and produced comparable amounts of TNF and TGF-β1 in both WT and *Trem1*$^{-/-}$ CCl_4-treated mice. Strikingly, *Trem1*-sufficient Kupffer cells could recruit patrolling monocytes into peripheral blood and inflammatory infiltrating monocytes into the livers of *Trem1*$^{-/-}$ mice. Recently, new players in TGF-β1–mediated liver fibrogenesis have been discovered, one of which is the Notch signaling pathway (46, 47). Notch pathway components were found to be significantly upregulated in TGF-β1-activated HSCs, inflammatory monocytes, macrophages and in mouse and human fibrotic livers (47). Our data demonstrated that TREM-1-positive Kupffer cells significantly upregulated the expression of a Notch ligand (*Jag1*) at an early stage of liver injury, supporting that Notch signaling in Kupffer cells may drive liver fibrosis by promoting cross-talk between Kupffer cells and HSCs. Although TGF-β1 is the major regulator of fibrogenesis, TGF-β1–independent pathways may also be involved. These new pathways include the emerging role of Oncostatin M (OSM), an inflammatory

cytokine of the IL-6 family that has been discovered in macrophage activation and lung fibrogenesis (48). Our data indicate a link between expression of *Osm* and TREM-1 signaling in Kupffer cells, which supports the concept that OSM from Kupffer cells may contribute to liver fibrogenesis.

Our data demonstrate that the TREM-1 pathway on Kupffer cells plays an essential role in hepatic inflammation and fibrogenesis in a mouse model of fibrosis. Furthermore, analysis of human liver tissue samples demonstrated robustly increased infiltration of TREM-1-positive Kupffer cells and monocytes/macrophages in fibrotic areas of patients with liver fibrosis. Therefore, interference with the functions of TREM-1 on Kupffer cells could provide a promising therapeutic approach, enabling the treatment of an overwhelming inflammatory liver response and fibrotic liver disease. Because several fibrogenic pathways are conserved across tissues, our findings on the role of TREM-1 in liver tissue-resident macrophages could be expanded to the study of fibrosis in the lungs, the heart, the kidneys and other organs.

Methods

Animals and fibrosis induction. Trem1-deficient mice were generated in our laboratory. Liver fibrosis was induced by CCl_4 peritoneal injection. See Supplemental methods for details.

Measurement of hepatic collagen deposition and cell infiltration. Collagen deposition was measured with Sirius Red Stain Kit or Masson Trichrome staining, and cell infiltration was measured by hematoxylin and eosin (H&E). See Supplemental methods for details.

Immunofluorescence, immunohistochemistry, staining with multiplex Opal method and thyramide signal amplification (TSA) plus fluorescent reagents, real time quantitative PCR and immunoblotting. These assays were performed by standard procedures. For more information, see Supplemental methods.

Assessment of alanine aminotransferase (ALT) and aspartate aminotransferase (AST). Blood of WT and *Trem1*$^{-/-}$ mice treated with oil (control) or with CCl_4 was collected, and sera were extracted from blood. Serum ALT and AST levels were measured with colorimetric assay Liquid ALT (SGPT) and Liquid AST (SGOT) (Pointe Scientific, Canton, MI, USA) according to the manufacturer's recommendations.

Isolation of bone marrow cells, liver non-parenchymal cells, and Kupffer cells from mice. Bone marrow cells were isolated from mouse femurs. Liver non-parenchymal cells and Kupffer cells were isolated by collagenase digestion in vivo, followed by further collagenase digestion in vitro. Cells were isolated by density gradient centrifugation followed by MACS magnetic bead separation. See Supplemental methods for details.

Isolation of hepatic stellate cells (HSCs). HSCs were isolated by in vivo digestion with a mixture of collagenase/pronase and further digested in vitro followed by density gradient centrifugation. See Supplemental methods for details.

Antibodies and flow cytometry analysis. Cells from bone marrow and blood and non-parenchymal cells from mouse liver were isolated and labeled with different antibodies. For more information concerning antibodies and staining conditions, see Supplemental methods.

RNA sequencing and data analysis. Total RNA from Kupffer cells was extracted using TRIzol® (Thermo Fisher Scientific, Waltham, MA, USA), and RNA sequencing and analysis were performed. For more information, see Supplemental methods. RNA sequencing data were deposited in the NCBI's Gene Expression Omnibus database (GEO GSE116236).

Depletion and adoptive transfer of Kupffer cells. Depletion of Kupffer cells was performed with clodronate-containing liposome suspension in *Trem1*-deficient mice. Kupffer cells from WT mice were isolated and adoptively transferred to recipient *Trem1*-deficient mice. For more information, see Supplemental methods.

Quantitative assessment of uptake and distribution of reticulo-endothelial system-specific nanoparticles during liver fibrogenesis. This assay was performed with Mvivo BIS nanoparticles and a small animal CT scanner. See Supplemental methods for details.

Human tissue. De-identified, formalin-fixed, paraffin-embedded liver tissue specimens from healthy controls (n = 6) and patients with liver fibrosis (n = 5) were obtained through US Biomax, Inc. (Rockville, MD, USA) and the Georgia Cancer Center Biorepository (Augusta, GA, USA). Liver fibrosis was evaluated according to Metavir staging. Significant fibrosis was defined as Metavir stages F≥2, severe fibrosis as Metavir F≥3, and cirrhosis as F4 (49). Masson Trichrome, fluorescent-multiplexed immunohistochemistry staining of human liver specimens and analysis is described in Supplemental methods.

Statistics. All data represent the mean ± SEM. Comparisons of 2 groups were analyzed using an unpaired, 2-tailed Student *t* test. Comparisons of 3 or more groups were analyzed using ANOVA with a Bonferroni's test when making multiple pair-wise comparisons between different groups. *p* values less than 0.05 were considered significant in all analyses. Analyses were performed using GraphPad Prism Software (GraphPad Software, Inc., La Jolla, CA, USA). For human liver samples, statistical analysis was performed using a statistical software package (SAS 9.4 software, SAS Institute Inc., Cary, NC, USA). One-way ANOVA analysis with Bonferroni's correction was used when making multiple pair-wise comparisons between 3 human-related groups after adjusting for multiplicity. As an exploratory analysis, least squared mean (LSM) testing was used to test the difference between any pair of subjects. *p*-values less than 0.05 were considered to be statistically significant.

Study approval. All mice were maintained under specific pathogen-free conditions at Augusta University according to IACUC protocol 2008-0051. Animal studies were performed in strict accordance with the recommendations in the NIH *Guide for the Care and Use of Laboratory Animals* (National Academy Press, 2011). Analysis of human formalin-fixed, paraffin-embedded tissue specimens was approved by the Augusta University Institutional Review Board, protocol 1023370.

Authors' contributions:

A.A., V.P.D., D.D.H., and A.D. designed and conducted experiments and analyzed results; A.S.A. provided support with image acquisition and analysis; R.S. analyzed results; A.T.N.L., G.T. and A.H. designed and conducted experiments, analyzed results and wrote the manuscript.

Acknowledgments

This work was supported by NIH grant CA172230 to A.H. We thank Dr. R.B. Markowitz for critical reading of the manuscript. We thank Dr. Houssein Abdul Sater, Dr. Roni Bollag and Ms. Kimya Jones of the Georgia Cancer Center Biorepository for helping to obtain liver samples and excellent technical support. We also thank Dr. Maciej Zerkowski (Perkin Elmer, New York, NY, USA) for technical advice to analyze multispectral images and phenotype of cells. We are grateful to the Georgia Cancer Center community for fruitful discussion and support.

References

1. Bataller R, and Brenner DA. Liver fibrosis. *The Journal of clinical investigation.* 2005;115(2):209-18.
2. Hernandez-Gea V, and Friedman SL. Pathogenesis of liver fibrosis. *Annual review of pathology.* 2011;6(425-56.
3. Bataller R, and Gao B. Liver fibrosis in alcoholic liver disease. *Seminars in liver disease.* 2015;35(2):146-56.
4. Schwabe R, and Bataller R. Liver fibrosis. Foreword. *Seminars in liver disease.* 2015;35(2):95-6.
5. Rosselli M, Lotersztajn S, Vizzutti F, Arena U, Pinzani M, and Marra F. The metabolic syndrome and chronic liver disease. *Current pharmaceutical design.* 2014;20(31):5010-24.
6. Koyama Y, and Brenner DA. Liver inflammation and fibrosis. *The Journal of clinical investigation.* 2017;127(1):55-64.
7. Akira S, and Takeda K. Toll-like receptor signalling. *Nature reviews Immunology.* 2004;4(7):499-511.
8. Adams DH, Ju C, Ramaiah SK, Uetrecht J, and Jaeschke H. Mechanisms of immune-mediated liver injury. *Toxicological sciences : an official journal of the Society of Toxicology.* 2010;115(2):307-21.
9. Woolbright BL, and Jaeschke H. The Impact of Sterile Inflammation in Acute Liver Injury. *Journal of clinical and translational research.* 2017;3(Suppl 1):170-88.

10. Tomasek JJ, Gabbiani G, Hinz B, Chaponnier C, and Brown RA. Myofibroblasts and mechano-regulation of connective tissue remodelling. *Nature reviews Molecular cell biology.* 2002;3(5):349-63.

11. Kubes P, and Mehal WZ. Sterile inflammation in the liver. *Gastroenterology.* 2012;143(5):1158-72.

12. Woolbright BL, and Jaeschke H. Sterile inflammation in acute liver injury: myth or mystery? *Expert review of gastroenterology & hepatology.* 2015;9(8):1027-9.

13. Seki E, De Minicis S, Osterreicher CH, Kluwe J, Osawa Y, Brenner DA, and Schwabe RF. TLR4 enhances TGF-beta signaling and hepatic fibrosis. *Nature medicine.* 2007;13(11):1324-32.

14. Wynn TA, and Ramalingam TR. Mechanisms of fibrosis: therapeutic translation for fibrotic disease. *Nature medicine.* 2012;18(7):1028-40.

15. Ford JW, and McVicar DW. TREM and TREM-like receptors in inflammation and disease. *Current opinion in immunology.* 2009;21(1):38-46.

16. Bouchon A, Dietrich J, and Colonna M. Cutting edge: inflammatory responses can be triggered by TREM-1, a novel receptor expressed on neutrophils and monocytes. *Journal of immunology.* 2000;164(10):4991-5.

17. Bouchon A, Facchetti F, Weigand MA, and Colonna M. TREM-1 amplifies inflammation and is a crucial mediator of septic shock. *Nature.* 2001;410(6832):1103-7.

18. Lanier LL. Natural killer cell receptor signaling. *Current opinion in immunology.* 2003;15(3):308-14.

19. Turnbull IR, and Colonna M. Activating and inhibitory functions of DAP12. *Nature reviews Immunology.* 2007;7(2):155-61.

20. Liao R, Sun TW, Yi Y, Wu H, Li YW, Wang JX, Zhou J, Shi YH, Cheng YF, Qiu SJ, et al. Expression of TREM-1 in hepatic stellate cells and prognostic value in

hepatitis B-related hepatocellular carcinoma. *Cancer science.* 2012;103(6):984-92.

21. Wu J, Li J, Salcedo R, Mivechi NF, Trinchieri G, and Horuzsko A. The proinflammatory myeloid cell receptor TREM-1 controls Kupffer cell activation and development of hepatocellular carcinoma. *Cancer research.* 2012;72(16):3977-86.

22. Pierce RA, Glaug MR, Greco RS, Mackenzie JW, Boyd CD, and Deak SB. Increased procollagen mRNA levels in carbon tetrachloride-induced liver fibrosis in rats. *The Journal of biological chemistry.* 1987;262(4):1652-8.

23. Oumi N, Taniguchi KA, Kanai AM, Yasunaga M, Nakanishi T, and Sato K. A crucial role of bone morphogenetic protein signaling in the wound healing response in acute liver injury induced by carbon tetrachloride. *International journal of hepatology.* 2012;2012(476820.

24. Friedman SL. Hepatic fibrosis -- overview. *Toxicology.* 2008;254(3):120-9.

25. Mann DA, and Marra F. Fibrogenic signalling in hepatic stellate cells. *Journal of hepatology.* 2010;52(6):949-50.

26. Mederacke I, Dapito DH, Affo S, Uchinami H, and Schwabe RF. High-yield and high-purity isolation of hepatic stellate cells from normal and fibrotic mouse livers. *Nature protocols.* 2015;10(2):305-15.

27. Mederacke I, Hsu CC, Troeger JS, Huebener P, Mu X, Dapito DH, Pradere JP, and Schwabe RF. Fate tracing reveals hepatic stellate cells as dominant contributors to liver fibrosis independent of its aetiology. *Nature communications.* 2013;4(2823.

28. McCay PB, Lai EK, Poyer JL, DuBose CM, and Janzen EG. Oxygen- and carbon-centered free radical formation during carbon tetrachloride metabolism.

Observation of lipid radicals in vivo and in vitro. *The Journal of biological chemistry.* 1984;259(4):2135-43.

29. El Mezayen R, El Gazzar M, Seeds MC, McCall CE, Dreskin SC, and Nicolls MR. Endogenous signals released from necrotic cells augment inflammatory responses to bacterial endotoxin. *Immunology letters.* 2007;111(1):36-44.

30. Brenner C, Galluzzi L, Kepp O, and Kroemer G. Decoding cell death signals in liver inflammation. *Journal of hepatology.* 2013;59(3):583-94.

31. Thankam FG, Dilisio MF, Dietz NE, and Agrawal DK. TREM-1, HMGB1 and RAGE in the Shoulder Tendon: Dual Mechanisms for Inflammation Based on the Coincidence of Glenohumeral Arthritis. *PloS one.* 2016;11(10):e0165492.

32. Subramanian S, Pallati PK, Sharma P, Agrawal DK, and Nandipati KC. Significant association of TREM-1 with HMGB1, TLRs and RAGE in the pathogenesis of insulin resistance in obese diabetic populations. *American journal of translational research.* 2017;9(7):3224-44.

33. Li L, Huang L, Sung SS, Vergis AL, Rosin DL, Rose CE, Jr., Lobo PI, and Okusa MD. The chemokine receptors CCR2 and CX3CR1 mediate monocyte/macrophage trafficking in kidney ischemia-reperfusion injury. *Kidney international.* 2008;74(12):1526-37.

34. Tacke F, Alvarez D, Kaplan TJ, Jakubzick C, Spanbroek R, Llodra J, Garin A, Liu J, Mack M, van Rooijen N, et al. Monocyte subsets differentially employ CCR2, CCR5, and CX3CR1 to accumulate within atherosclerotic plaques. *The Journal of clinical investigation.* 2007;117(1):185-94.

35. Deleve LD, Wang X, and Guo Y. Sinusoidal endothelial cells prevent rat stellate cell activation and promote reversion to quiescence. *Hepatology.* 2008;48(3):920-30.

36. DeLeve LD. Liver sinusoidal endothelial cells and liver regeneration. *The Journal of clinical investigation.* 2013;123(5):1861-6.

37. Trautwein C, Friedman SL, Schuppan D, and Pinzani M. Hepatic fibrosis: Concept to treatment. *Journal of hepatology.* 2015;62(1 Suppl):S15-24.

38. Fallowfield JA. Future mechanistic strategies for tackling fibrosis--an unmet need in liver disease. *Clinical medicine.* 2015;15 Suppl 6(s83-7.

39. Marra F, Aleffi S, Galastri S, and Provenzano A. Mononuclear cells in liver fibrosis. *Seminars in immunopathology.* 2009;31(3):345-58.

40. Marra F, and Tacke F. Roles for chemokines in liver disease. *Gastroenterology.* 2014;147(3):577-94 e1.

41. Klesney-Tait J, Keck K, Li X, Gilfillan S, Otero K, Baruah S, Meyerholz DK, Varga SM, Knudson CJ, Moninger TO, et al. Transepithelial migration of neutrophils into the lung requires TREM-1. *The Journal of clinical investigation.* 2013;123(1):138-49.

42. Kolaczkowska E, and Kubes P. Neutrophil recruitment and function in health and inflammation. *Nature reviews Immunology.* 2013;13(3):159-75.

43. Stock AT, Smith JM, and Carbone FR. Type I IFN suppresses Cxcr2 driven neutrophil recruitment into the sensory ganglia during viral infection. *The Journal of experimental medicine.* 2014;211(5):751-9.

44. Rydstrom A, and Wick MJ. Monocyte and neutrophil recruitment during oral Salmonella infection is driven by MyD88-derived chemokines. *European journal of immunology.* 2009;39(11):3019-30.

45. Koyama Y, Wang P, Liang S, Iwaisako K, Liu X, Xu J, Zhang M, Sun M, Cong M, Karin D, et al. Mesothelin/mucin 16 signaling in activated portal fibroblasts regulates cholestatic liver fibrosis. *The Journal of clinical investigation.* 2017;127(4):1254-70.

46. Geisler F, and Strazzabosco M. Emerging roles of Notch signaling in liver disease. *Hepatology.* 2015;61(1):382-92.

47. Bansal R, van Baarlen J, Storm G, and Prakash J. The interplay of the Notch signaling in hepatic stellate cells and macrophages determines the fate of liver fibrogenesis. *Scientific reports.* 2015;5(18272.

48. Wong S, Botelho FM, Rodrigues RM, and Richards CD. Oncostatin M overexpression induces matrix deposition, STAT3 activation, and SMAD1 Dysregulation in lungs of fibrosis-resistant BALB/c mice. *Laboratory investigation; a journal of technical methods and pathology.* 2014;94(9):1003-16.

49. Boursier J, de Ledinghen V, Zarski JP, Rousselet MC, Sturm N, Foucher J, Leroy V, Fouchard-Hubert I, Bertrais S, Gallois Y, et al. A new combination of blood test and fibroscan for accurate non-invasive diagnosis of liver fibrosis stages in chronic hepatitis C. *The American journal of gastroenterology.* 2011;106(7):1255-63.

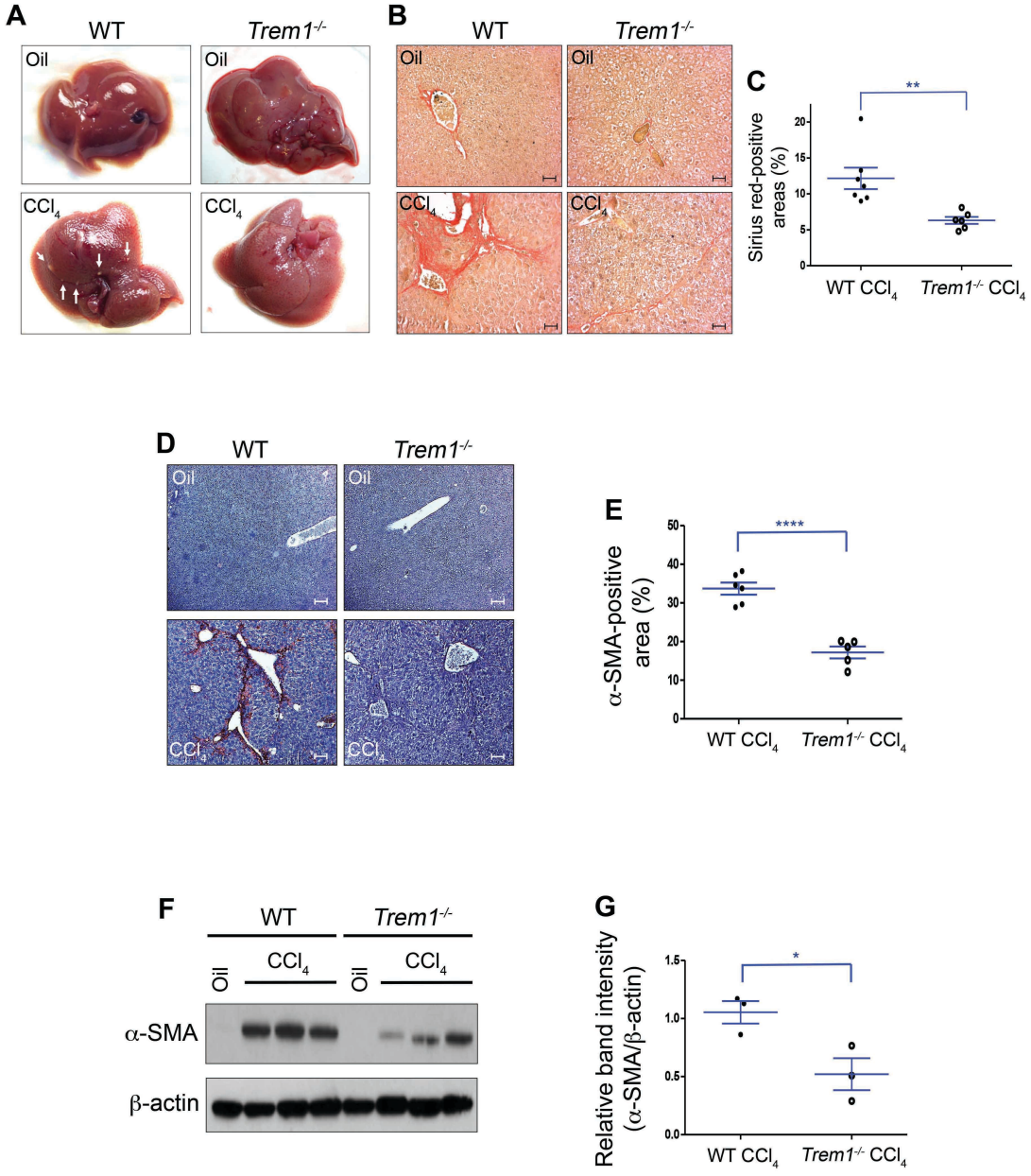

Figure 1. Deletion of *Trem1* attenuates hepatic fibrogenesis. (**A**) Representative macroscopic pictures of livers from WT and *Trem1*$^{-/-}$ control mice (oil-injected, n = 3 per group, upper panels) and from WT and *Trem1*$^{-/-}$ mice treated with 12 injections (6 weeks) of CCl_4 (n = 6-7 per group, lower panels). Arrowheads indicate fibrotic nodules visible on CCl_4-treated WT mice. (**B**) Collagen deposition was evaluated by Sirius red

staining. Representative images of liver sections from WT and *Trem1*$^{-/-}$ control (n = 3 per group, upper panels) and from WT and *Trem1*$^{-/-}$ mice treated with CCl_4 (n = 6-7 per group, lower panels, original magnification, x20; scale bars, 50 μm). (**C**) Quantification of Sirius red-positive areas (%). (**D**) Representative images of liver sections from WT and *Trem1*$^{-/-}$ control (n = 3 per group, upper panels) and from WT and *Trem1*$^{-/-}$ mice treated with CCl_4 (n = 5-6 per group, lower panels) stained with anti-α-SMA antibody (original magnification, x10; scale bars, 100 μm). (**E**) Quantification of α-SMA-positive areas (%). (**F**) Immunoblot analysis for α-SMA in liver lysates from the indicated mice (n = 3 per group). β-actin was used as loading control. (**G**) Quantification of α-SMA expression (n = 3 mice per group). Results are displayed as mean ± SEM. *$p < 0.05$, **$p < 0.01$, ****$p < 0.0001$. Two-tailed Student's *t* test was used in **C**, **E** and **G**. Experiments shown in **A**, **B** and **D** are representative of 2 independent experiments.

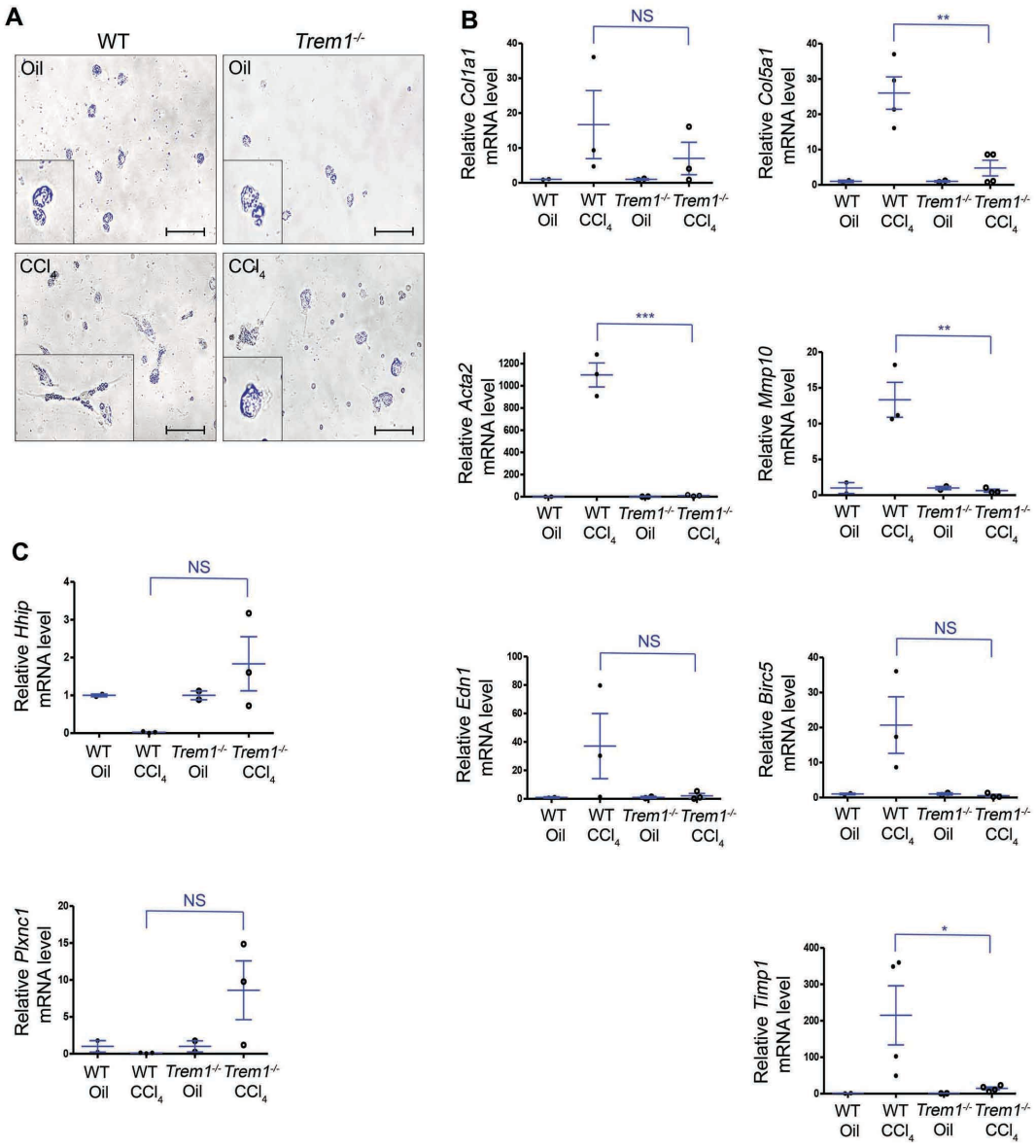

Figure 2. Deletion of *Trem1* attenuates HSC activation and differentiation. HSCs were isolated from control (oil-injected) WT and *Trem1*$^{-/-}$ (n = 3 per group) and WT and *Trem1*$^{-/-}$ mice (n = 3-4 per group) treated with CCl_4 for 6 weeks. (**A**) Representative images of freshly isolated HSCs from indicated mice (oil-injected, upper panels and CCl_4-treated, lower panels), visualized using a merge of phase-contrast microscopy and retinoid fluorescence (blue channel), show that HSCs from WT CCl_4-injured mice

differentiated into myofibroblasts and lost their retinoic acid droplets (original magnification, x40. Scale bars, 25 µm). Experiments shown here are representative of 2 independent experiments. (**B**, **C**) Total RNA was isolated from HSC fractions of WT or *Trem1*$^{-/-}$ mice (n = 3-4 per group) treated with CCl_4 for 6 weeks. *Col1a1*, *Col5a1*, *Acta2*, *Mmp10*, *Edn1*, *Birc5*, *Timp1*, *Hhip* and *Plxnc1* mRNA levels were determined by RT-qPCR and represented as fold-induction. Results are displayed as mean ± SEM. *$p < 0.05$, **$p < 0.01$, ***$p < 0.001$. Two-tailed Student's *t* test was used.

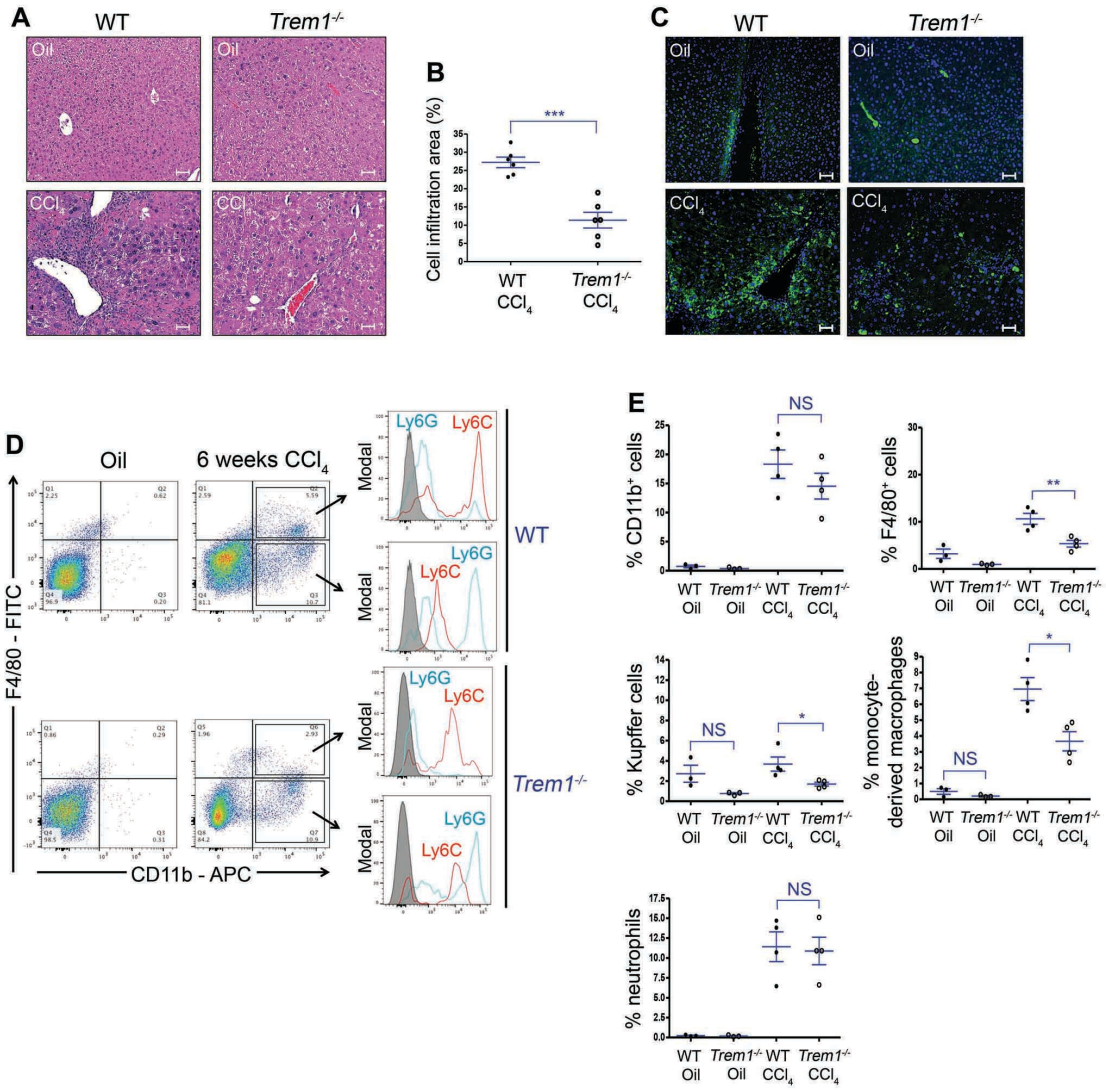

Figure 3. TREM-1 is essential for recruitment and differentiation of monocyte-derived macrophages during hepatic fibrogenesis. WT and *Trem1*$^{-/-}$ mice were treated with 12 injections of CCl_4 (6 weeks). (**A**) Representative images of liver sections stained with H&E from WT and *Trem1*$^{-/-}$ control (oil-injected, n = 3 per group, upper panels) and from WT and *Trem1*$^{-/-}$ (n = 6 per group) CCl_4-injured mice (lower panels). Histology images reveal important mononuclear cell infiltration of fibrotic livers (original magnification, x20. Scale bars, 50 µm). (**B**) Quantification of cell infiltration areas (%). (**C**) Representative images of liver sections stained with FITC-conjugated anti-F4/80

antibody from control (n = 3 per group, upper panels) and CCl_4-injured mice (n = 6-7 per group, lower panels, original magnification, x20. Scale bars, 50 µm). (**D**) Flow cytometry dot plots of cells for identification of Kupffer cells ($F4/80^+$-$CD11b^-$), monocyte-derived macrophages ($F4/80^+$-$CD11b^+$-$Ly6C^{high}$-$Ly6G^{low}$) and neutrophils ($F4/80^-$-$CD11b^+$-$Ly6G^{high}$-$Ly6C^{low}$) in liver from control WT and *Trem1*$^{-/-}$ mice (n = 3 per group), and from CCl_4-injured WT and *Trem1*$^{-/-}$ mice (n = 4 per group). Control staining was performed with IgG isotype (grey histograms). (**E**) Percentage of liver-infiltrated cell populations in WT and *Trem1*$^{-/-}$ mice, analyzed by flow cytometry, after 6 weeks oil or CCl_4 treatment. Results are displayed as mean ± SEM. $*p < 0.05$, $**p < 0.01$, $***p < 0.001$. Two-tailed Student's *t* test was used in **B** and **E**. Experiments shown in **A** and **C** are representative of 2 independent experiments.

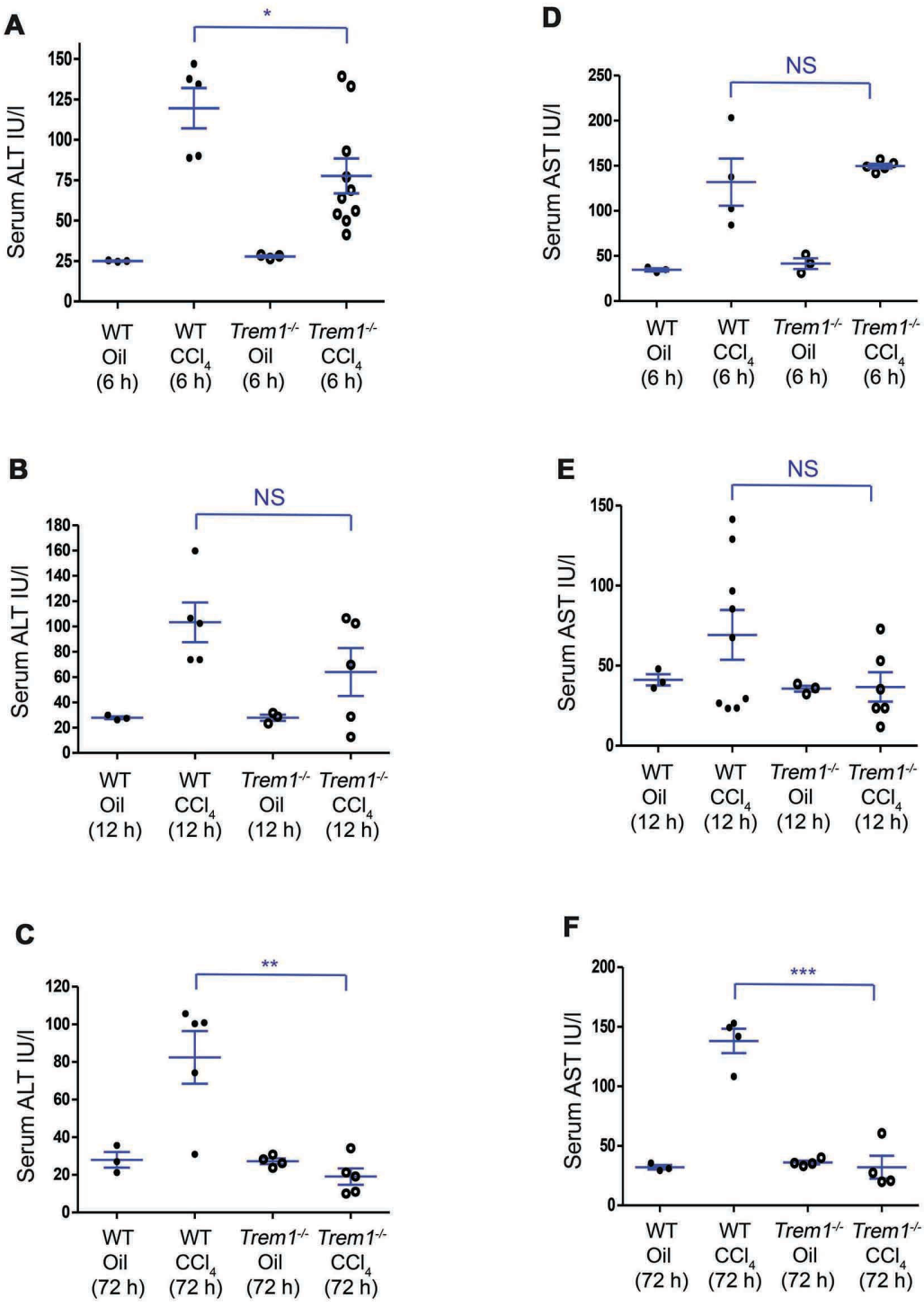

Figure 4. Deletion of *Trem1* decreases liver injury at early stages of liver fibrogenesis. WT and *Trem1*$^{-/-}$ mice were analyzed 6 h, 12 h, and 72 h after injection of single dose of CCl_4. Serum ALT (**A-C**) and AST (**D-F**) levels from indicated mice were

measured with colorimetric assay (n = 3-10 mice/time-point/group). Results are displayed as mean ± SEM. *$p < 0.05$, **$p < 0.01$, ***$p < 0.001$. Two-tailed Student's *t* test was used.

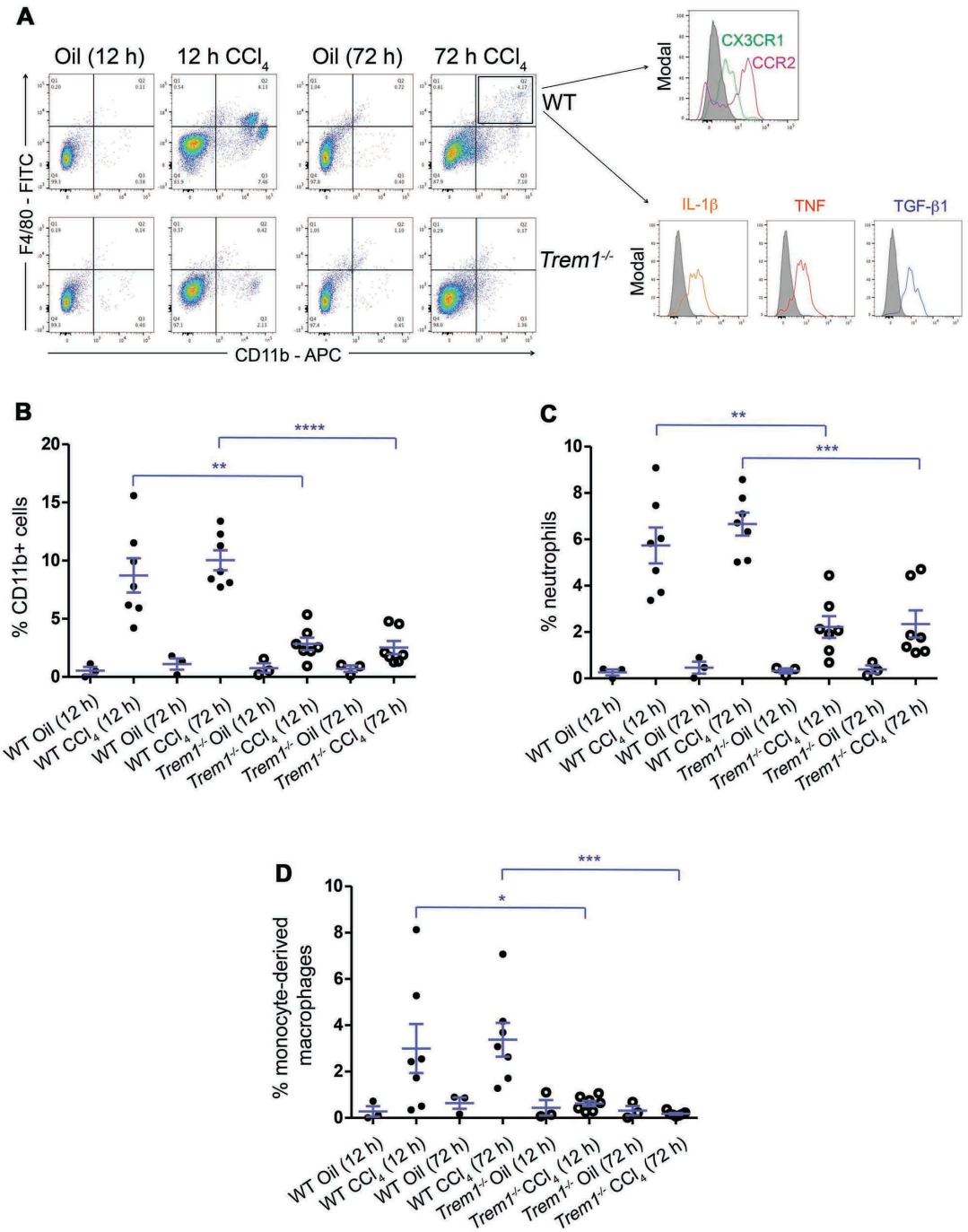

Figure 5. Deletion of *Trem1* reduces inflammatory cell infiltration at early stages of liver fibrogenesis. (**A**) Flow cytometry dot plots of liver cells from control WT and *Trem1*$^{-/-}$ mice (oil-injected, n = 3 per group), and from WT and *Trem1*$^{-/-}$ mice 12 h and 72 h after CCl_4 injury (n = 7 mice/time-point/group) stained with anti-F4/80, anti-CD11b,

anti-CCR2, anti-CX3CR1, anti-IL-1β, anti-TNF and anti-TGF-β1 antibodies. Liver cells from WT mice were stained and analyzed 72 h after CCl_4 injection for the expression of CCR2 and CX3CR1 (n = 5 mice) and for the intracellular expression of IL-1β, TNF and TGF-β1 (n = 7 mice). Flow cytometry histograms represent cells gated on $F4/80^+$-$CD11b^+$ population. Control staining was performed with IgG isotype (grey histograms). (**B-D**) Percentage of $CD11b^+$ cells, neutrophils, and inflammatory monocyte-derived macrophages in liver from WT and *Trem1*$^{-/-}$ mice, quantified after 12 h and 72 h oil (n = 3 mice/time-point/group) or CCl_4 treatment (n = 7 mice/time-point/group). Results are displayed as mean ± SEM. *$p < 0.05$, **$p < 0.01$, ***$p < 0.001$, ****$p < 0.0001$. Two-tailed Student's *t* test was used in **B, C** and **D**.

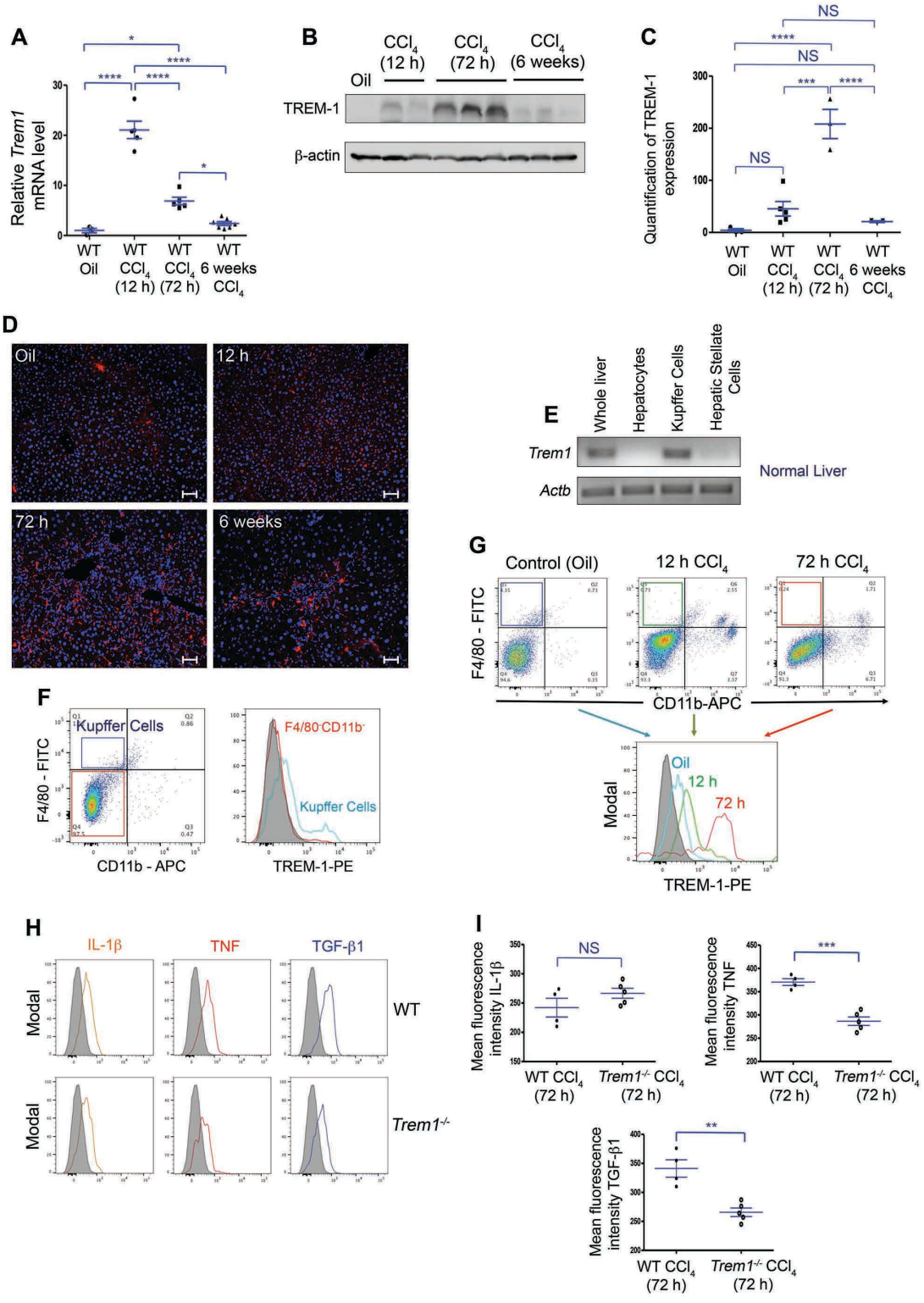

Figure 6. Expression of *Trem1* in liver during fibrogenesis. (**A**) WT mice were treated with oil (control, n = 3) or with a single dose of CCl_4 and analyzed after 12 h and

72 h (n = 5 mice/time-point). Another group of WT mice were treated with 12 injections of CCl_4 and analyzed after 6 weeks of treatment (n = 7 mice). mRNA levels of *Trem1* from livers assessed by RT-qPCR. Expression is normalized to the average of 3 different control genes (*Actb*, *Gapdh* and *Hprt1*) and represented as fold-induction. (**B**) Representative immunoblot analysis for TREM-1 in liver lysates from WT mice with different time-points. β-actin was used as loading control. (**C**) Quantification of TREM-1 expression in liver of WT control mice (n = 3) and 12 h (n = 5), 72 h (n = 3) and 6 weeks (n = 3) CCl_4-treated mice. (**D**) Representative images of immunofluorescence staining of liver sections with phycoerythrin (PE)-conjugated anti-TREM-1 antibody from WT control mice (oil-injected, n = 3) and 12 h (upper panels), 72 h and 6 weeks CCl_4-treated mice (n = 5-7 mice/time-point/group, lower panels original magnification, x20. Scale bars, 50 μm). Experiments shown here are representative of 2 independent experiments. (**E**) *Trem1* mRNA expression assessed by PCR from whole liver, purified hepatocyte, Kupffer cell and HSC fractions of WT mice (n = 3 mice/cell fraction). (**F**) Flow cytometry dot plots of liver cells from WT control mice (n = 9) stained with anti-F4/80 and anti-CD11b antibodies. Flow cytometry histograms represent TREM-1 expression, on gated $F4/80^-$-$CD11b^-$ cell population and on gated $F4/80^+$-$CD11b^-$ Kupffer cells (n = 9 mice). Control staining was performed with IgG isotype (grey histogram). (**G**) Flow cytometry dot plots and histograms of TREM-1 expression, on gated $F4/80^+$-$CD11b^-$ Kupffer cells, isolated from WT control (oil-injected, n = 9), 12 h and 72 h CCl_4-injured mice (n = 7 mice/time-point/group). Control staining was performed with IgG isotype (grey histogram). (**H**) Flow cytometry histograms of intracellular expression of IL-1β, TNF and TGF-β1 on gated $F4/80^+$-$CD11b^-$ Kupffer cells from 72 h CCl_4-injured WT (n = 4) and $Trem1^{-/-}$ mice (n = 5). Control staining was performed with IgG isotype (grey histograms). (**I**) Quantification of mean fluorescence intensity of indicated cytokines. Results are displayed as mean ± SEM. *$p < 0.05$, **$p < 0.01$, ***$p < 0.001$, ****$p < 0.0001$. ANOVA

followed by Bonferroni's post hoc test was used in **A** and **C**. Two-tailed Student's *t* test was used in **I**.

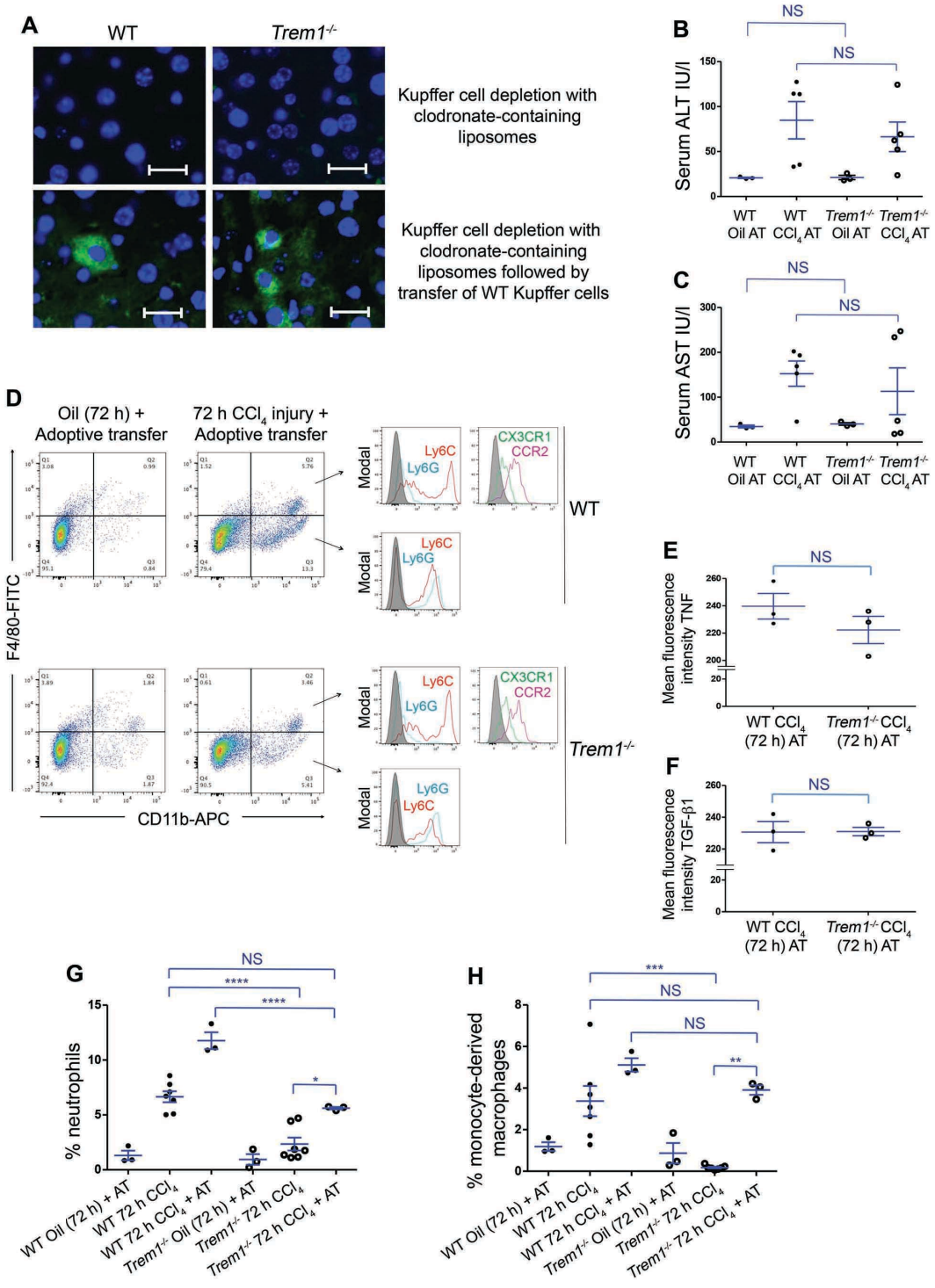

Figure 7. Adoptive transfer (AT) of Kupffer cells from WT mice increases liver injury and recruitment of inflammatory cells in *Trem1*$^{-/-}$ mice. (**A**) Representative images of liver sections from indicated mice stained with FITC-conjugated anti-F4/80

antibody 72 h after injection of clodronate-containing liposomes (n = 3 mice per group, upper panels) followed by reconstitution of pre-depleted livers with WT Kupffer cells (n = 3 mice per group). Adoptively transferred cells were observed at 72 h by immunofluorescence staining (original magnification, x40. Scale bars, 20 μm). Experiments shown here are representative of 2 independent experiments. (**B**) Serum ALT and (**C**) AST levels from WT and *Trem1*$^{-/-}$ mice with adoptive transfer of WT Kupffer cells followed by a single dose of CCl_4 treatment were measured at 72 h post CCl_4 injury with colorimetric assay (n = 3-5 mice per group). (**D**) Macrophage-depleted WT and *Trem1*$^{-/-}$ mice were adoptively transferred with WT Kupffer cells following treatment with a single dose of CCl_4. Flow cytometry dot plots of liver cells stained with anti-F4/80, anti-CD11b, anti-TNF, anti-TGF-β1, anti-Ly6C, anti-Ly6G, anti-CCR2 and anti-CX3CR1 antibodies (n = 3 mice per group). Flow cytometry histograms of Ly6C, Ly6G, CCR2 and CX3CR1 expression shown on gated F4/80^{+}-CD11b^{+} and F4/80^{-}-CD11b^{+} cells (n = 3 mice per group). Control staining was performed with IgG isotype (grey histograms). Mean fluorescence intensity of TNF (**E**) and TGF-β1 (**F**) in indicated mice shown on gated F4/80^{+}-CD11b^{-} Kupffer cells (n = 3 mice per group). (**H** and **I**) Percentage of liver-infiltrated neutrophils and inflammatory monocytes in indicated experimental conditions in WT and *Trem1*$^{-/-}$ mice (n = 3-7 per group). Results are displayed as mean ± SEM. ***p* < *0.01*, ****p* < *0.001*, *****p* < *0.0001*. Two-tailed Student's *t* test was used in **B**, **C**, **E** and **F**. ANOVA followed by Bonferroni's post hoc test was used in **G** and **H**.

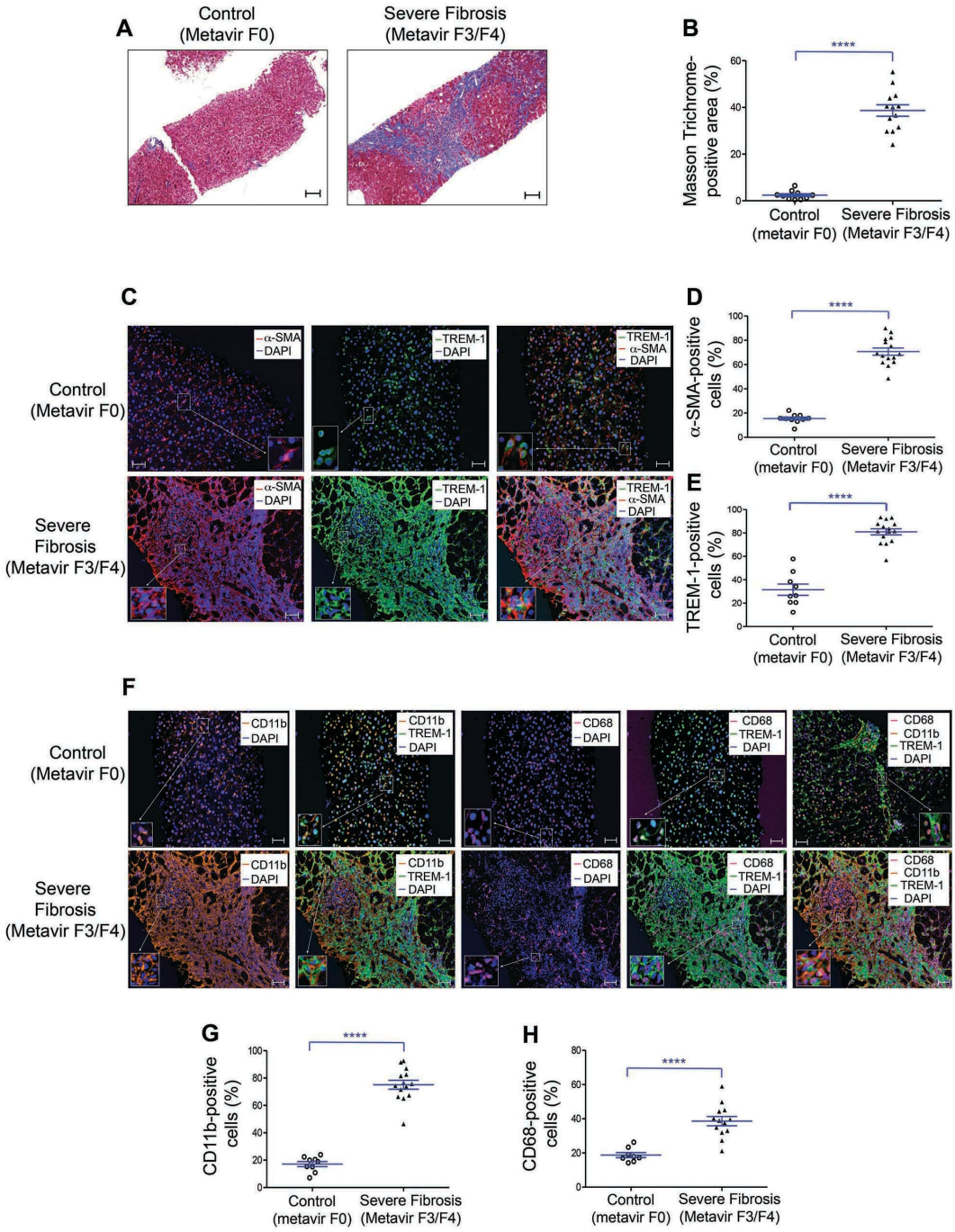

Figure 8. Increased TREM-1-, CD11b-, and CD68-positive cell infiltration in human liver samples from patients diagnosed with advanced fibrosis. (**A**) Representative images of human liver samples from control (Metavir = F0, n = 6) and a patient diagnosed with advanced fibrosis (Metavir = F3/F4, n = 4) stained with Masson

Trichrome for collagen deposition (original magnification, x10; scale bar, 100 μm). (**B**) Quantification of Masson Trichrome-positive areas (%) from control (n = 10 areas) and a patient with advanced fibrosis (n = 13 areas). (**C**) Fluorescent-multiplexed immunohistochemistry of human liver samples. Samples from control and a patient with advanced fibrosis were stained for α-SMA (red), TREM-1 (green) and DAPI (blue) (original magnification, x20; scale bar, 50 μm). (**D**) Quantification of α-SMA-positive cells (%) from control and a patient with advanced fibrosis (n = 10 areas *vs* n = 15 areas, respectively. (**E**) Quantification of TREM-1-positive cells (%) from control and a patient with advanced fibrosis (n = 9 and n = 14 areas, respectively). (**F**) Samples from control and a patient with advanced fibrosis were stained for CD11b (orange), CD68 (magenta), TREM-1 (green) and DAPI (blue) (original magnification, x20; scale bar, 50 μm). (**G**) Quantification of CD11b-positive cells (%) from control and a patient with advanced fibrosis (n = 10 vs n = 15 areas, respectively). (**H**) Quantification of CD68-positive cells (%) from control and from patient with advanced fibrosis (n = 8 and n = 12 areas, respectively). All data shown are displayed as mean ± SEM. ****$p < 0.0001$. Two-tailed Student's *t* test was used in **B**, **D**, **E**, **G** and **H**.